Icarus 303 (2018) 34–46

Contents lists available at ScienceDirect

Icarus

journal homepage: www.elsevier.com/locate/icarus

Comparative ionospheres: Terrestrial and giant planets

Michael Mendillo[a], Jeffrey Trovato[a], Luke Moore[a,*], Ingo Müller-Wodarg[b]

[a] Center for Space Physics, Boston University, Boston, MA 02215, USA
[b] Department of Physics and Astronomy, Imperial College, London, UK

ARTICLE INFO

Article history:
Received 26 June 2017
Revised 4 December 2017
Accepted 20 December 2017
Available online 22 December 2017

ABSTRACT

The study of planetary ionospheres within our solar system offers a variety of settings to probe mechanisms of photo-ionization, chemical loss, and plasma transport. Ionospheres are a minor component of upper atmospheres, and thus their mix of ions observed depends on the neutral gas composition of their parent atmospheres. The same solar irradiance (x-rays and extreme-ultra-violet vs. wavelength) impinges upon each of these atmospheres, with solar flux magnitudes changed only by the inverse square of distance from the Sun. If all planets had the same neutral atmosphere—with ionospheres governed by photochemical equilibrium (production = loss)—their peak electron densities would decrease as the inverse of distance from the Sun, and any changes in solar output would exhibit coherent effects throughout the solar system.

Here we examine the outer planet with the most observations of its ionosphere (Saturn) and compare its patterns of electron density with those at Earth under the same-day solar conditions. We show that, while the average magnitudes of the major layers of molecular ions at Earth and Saturn are approximately in accord with distance effects, only minor correlations exist between solar effects and day-to-day electron densities. This is in marked contrast to the strong correlations found between the ionospheres of Earth and Mars. Moreover, the variability observed for Saturn's ionosphere (maximum electron density and total electron content) is much larger than found at Earth and Mars. With solar irradiance changes far too small to cause such effects, we use model results to explore the roles of other agents. We find that water sources from Enceladus at low latitudes, and 'ring rain' at middle latitudes, contribute substantially to variability via water ion chemistry. Thermospheric winds and electrodynamics generated at auroral latitudes are suggested causes of high latitude ionospheric variability, but remain inconclusive due to the lack of relevant observations.

1. Introduction

The defining characteristic of a planet's ionosphere is its profile of electron density versus height, $N_e(h)$. Given that all ionospheres in our solar system are produced by the same solar photon energy versus wavelength spectrum, it is not surprising that both terrestrial and giant planet ionospheres share similar morphological structures. Solar X-rays ($\lambda < 100$ A)—high in energy but low in flux—penetrate an atmosphere to lower altitudes to produce secondary regions of ionization. These are known by the labels E-layer at Earth, M1-layer at Mars, and S1-layer at Saturn. The Sun's EUV photons (ionizing between 100–1240 A) are lower in energy but more abundant, and they produce the primary F-layer, M2-layer and S2-layer at Earth, Mars and Saturn, respectively. The basic principles of ionospheric physics—the foundations for comparative aeronomy—are summarized in major textbooks (Rishbeth and Garriott, 1969; Schunk and Nagy, 2009) and in two research monographs (Mendillo et al., 2002; Nagy et al., 2008).

A key element of comparative ionospheric research is the realization that the Earth is the only planet in the solar system that has a peak plasma density composed of atomic ions (O^+) and electrons (e^-). All other planetary ionospheres in our solar system have mostly molecular ions at their altitudes of maximum plasma density—O_2^+ at Venus and Mars, and H_3^+ at Jupiter, Saturn, Uranus and Neptune. These molecular ion layers occur within dense neutral atmospheres and thus result from the dominance of photochemical equilibrium (PCE) —determined by the balance of photo-ionization and plasma recombination, without plasma dynamics.

Atomic ions do appear in other ionospheres, e.g. O^+ at Venus and Mars, and H^+ in the giant planet ionospheres, but these have

* Corresponding author.
E-mail address: moore@bu.edu (L. Moore).

https://doi.org/10.1016/j.icarus.2017.12.033

densities well below the planet's maximum electron density. These plasmas result from both PCE theory and plasma diffusion and do not appear as distinct permanent layers within the planet's topside ionospheres. The ionosphere at Earth changes from O^+ ions at the F-layer peak (h ~ 300 km) to H^+ ions at topside heights, leading to a plasmasphere without an additional layer. Below the F-layer at Earth, however, there is a PCE region of molecular ions (O_2^+, N_2^+, NO^+) that form a prominent secondary ionospheric layer (the E-region at ~110 km). Thus, spanning the solar system, comparative studies of ionospheric layers governed by PCE conditions must focus on the terrestrial E-layer versus the main layers at other planets.

Given this basic understanding of solar system ionospheres, present-day research deals with departures from "textbook" conditions. These fall primarily into categories associated with variable output from the Sun: (a) changes in the solar irradiance (photon flux versus wavelength) that occur with time-scales ranging from flares (~minutes) to sunspot cycles (~years), and (b) solar wind variability due to coronal mass ejections (~days) and rotating active regions (~monthly). While current studies of solar photon effects upon the terrestrial ionosphere use daily observations of soft X-rays and EUV radiation from the Sun, prior to such space-based capabilities researchers relied upon a ground-based proxy for solar output—the solar radio flux at 10.7 cm. Because this radio index (designated as F10.7) has a good average correlation with actual x-rays and EUV, daily values of F10.7 are still used in terrestrial studies of long-term effects, as well as for studies of ionospheres on other planets where no solar irradiance observations are made. The units for F10.7 are formally 10^{-22} W/m^2/Hz, but the common practice is to use their integer magnitudes that range from ~70 units at solar minimum to ~150–350 units at solar maximum. For this study will use F10.7 for these reasons.

In addition to ionospheric variations due to solar and solar wind external drivers, ionospheres also vary as a result of (c) changes in the neutral atmosphere associated with upward coupling of waves and tides from the lower to upper atmosphere, and (d) composition changes due to thermal expansion and varying atmospheric dynamics and circulation. Atmospheric waves, for example, have time scales ranging from ~minutes to ~hours, and the time scales for tidal effects and global circulation are diurnal (with sub-harmonics).

In this paper, we briefly review day-to-day changes in ionospheric morphologies on Earth and Mars to define methods of quantitatively assessing common variability patterns and sources. We then apply that approach to same-day observations on Earth and Saturn to explore inner versus outer solar system patterns of ionospheric variability. We conclude with model results that test possible sources of the observed variability magnitudes at Saturn.

2. Ionospheric variability on terrestrial planets

2.1. Earth

Sources of ionospheric variability have been well documented at Earth (e.g., Forbes et al., 2000; Rishbeth and Mendillo, 2001). The typical procedure has been to use radio reflection ("ionosonde") observations of mid-day electron density values spanning a month, and to characterize variability as the standard deviation [σ(%)] about the monthly mean value. For the maximum electron density of the F-layer (NmF2), the components of overall variability [σ_{total}] can be attributed to solar photon irradiance [σ_{sun}], solar-wind-induced geomagnetic activity [σ_{mag}], and meteorological coupling from below [σ_{met}]. The analysis method used by Rishbeth and Mendillo (2001) treated such contributions as independent functions. Following that approach, and guided by the numerical values used in Forbes et al. (2000) and Rishbeth and Mendillo (2001), we adopt as a general scheme that ionospheric variability about a monthly mean $< N_mF2 >$ under mid-day conditions can be portrayed as follows:

$$[\sigma_{total}]^2 = [\sigma_{sun}]^2 + [\sigma_{mag}]^2 + [\sigma_{met}]^2$$
$$[20-25\%]^2 \approx [3-6\%]^2 + [14-17\%]^2 + [14-17\%]^2 \quad (1)$$

An alternative way to monitor the terrestrial ionosphere is via observations utilizing trans-ionosphere radio beacons (e.g., using GPS satellites). This method provides the integral of the full electron density (N_e) profile—with total electron content defined as $TEC = \int N_e(h)\, dh$. Since most of this column content comes from the F-layer, TEC is highly correlated (≈90%) with NmF2 (Fox et al., 1991), and thus σ_{TEC}(%) is also 20–30% (Johansson et al., 1978). The overall message for both peak electron density and TEC is clear: the influence of solar irradiance is minimal in comparison to solar wind sources of downward coupling and neutral atmosphere sources of upward coupling—with the latter two being comparable. This simply restates the fact that the F-layer of the terrestrial ionosphere is not fully described by internal photochemical equilibrium (PCE) processes. Plasma dynamics (diffusion along magnetic field lines, neutral wind-coupling, electro-dynamics) compete with PCE, and changes in the thermosphere (waves and tides) affect the abundance of neutral gases that are ionized.

For a pure-PCE layer in the terrestrial ionosphere, variability is much less because of the absence of significant contributions from dynamical sources. This is the case for the E-layer. In their study of sources of E-layer variability, Moore et al. (2006b) used observations and modeling of mid-day conditions at mid-latitudes. Their finding for observed variability was

$$\sigma_{total}(\mathrm{NmE}) = 7-12\%. \quad (2)$$

The Moore et al. (2006b) modeling studies showed that the contribution from solar input (changes in flux and declination over a month) was 8–9%. The remaining contributions came from small changes in the neutral atmosphere. At high latitudes affected by unique auroral processes, variability could be as high as 50%. In summary, the dominance of the solar photon contribution to E-layer variability is opposite to the behavior found for the F-layer, as summarized by Eq. (1). The E-layer is thus the appropriate molecular ion layer of the Earth's ionosphere to compare with the major molecular ion-electron plasma layers found for all other planets in the solar system because they are all governed by photochemical equilibrium processes.

There is no consensus for the nomenclature of ionospheric layers beyond the Earth. Here we adopted the approach introduced by Rishbeth and Mendillo (2004) where layers at Mars were designated numerically from low to high altitudes—resulting in the M1-layer near 110 km and the M2-layer at ~130 km. In terms of electron density, the M1-layer has a maximum number density termed NmM1 that is less than the maximum plasma density above it (NmM2). These correspond to layers produced primarily by soft X-rays and extreme ultraviolet (EUV) photons, respectively. For Saturn, we use a similar terminology (NmS2) to designate the maximum electron density of the primary layer in Saturn's ionosphere.

2.2. Mars

The first study of ionospheric variability at Mars used Mars Global Surveyor (MGS) radio-occultation observations to examine NmM2 values extracted from N_e(h) profiles. The period 9–27 March 1999 was selected because Mars was in opposition, and thus the solar flux measured at Earth could be applied to Mars' distance (d) by a simple $1/d^2$ correction (Mendillo et al., 2003). The day-to-day variability over a 17-day period was $\sigma(N_mM2) = 5\%$. In a simulation study of the same observing period, Martinis et al. (2003) used a PCE model to compute N_e(h)

profiles, and the predicted variability of daily values of NmM2 was ~6%. Those simulations used the same neutral atmosphere for all 17 days, and thus the variability resulted purely from day-to-day changes in solar irradiance.

2.3. Earth versus Mars

2.3.1. Day-to-day effects

The same 9–27 March 1999 period of MGS observations when Mars was in opposition provided the first case-study of simultaneous ionospheric variability on two planets (Mendillo et al., 2003). Using ionosonde data at Earth, the variability of NmE for daytime conditions was $\sigma = 5$–10%, consistent with the Moore et al. (2006b) results. Thus, the M2-layer at Mars and the E-layer at Earth exhibited similar variability patterns during a brief period of observations that included significant fluctuations in solar activity.

2.3.2. Solar cycle effects

To address longer time scales, a recent study of NmM2-layer and E-layer observations spanning six years was described in Mendillo et al. (2016). For Mars, the MGS radio occultation data base was used to obtain daily values of NmM2 from 1 November 2001 to 9 June 2005. The solar radio flux ($F_{10.7}$) measured at Earth during this interval changed from solar maximum conditions (170 units) to solar minimum values (100 units). A total of 697 days of observations of NmM2 at Mars were then compared with ⟨NmE⟩ observations at Earth obtained by averaging observations from four ionosonde stations for the same solar conditions. The qualifier "same solar conditions" was achieved by the so-called "rotated sun" method: the side of the Sun facing Mars on a day of MGS observations faced the Earth on a different day that can be determined from the known rotation rate of the Sun and the orbital separations of Earth and Mars. For this rotated Sun date, observations from Earth are then used to achieve "same solar conditions" as experienced by MGS at Mars—assuming, of course, that solar activity did not change significantly during the days of rotation. These same-day observations at Earth and Mars were then converted to local noon conditions at equivalent circular orbits—achieved by using the PCE equations of *1/d* for distance effects on electron density and *[cos (SZA)]$^{1/2}$* for sub-solar corrections (SZA being the solar zenith angle). The results for equivalent sub-solar values of NmE at Earth (1 AU) and NmM2 at Mars (1.524 AU) are shown in Fig. 1. Note that neither solar irradiance values nor their radio flux proxy ($F_{10.7}$) are used in this method of comparison—but rather direct ionospheric observations under same-day solar conditions.

Fig. 1 shows a clear trend between the terrestrial and martian ionospheres over long time scales. While not a precise linear pattern, the Pearson linear correlation coefficient is still high (0.85). The correlation equation shown describes long term effects of solar irradiance changes over the portion of a solar cycle from maximum to minimum conditions. Within each period (A, B, C), the variability [σ(%)] about the average values of NmE and NmM2 were within the 4–8% range. We conclude that, while ionospheric layer magnitudes at Earth and Mars change by ~50% from solar cycle max-to-min epochs, their variability about average values remained relatively constant during changing solar cycle conditions. We now apply such methods of variability characterization to the ionosphere of Saturn.

3. Ionospheric variability on giant planets

3.1. Description of observations and data processing

Since 1979 there have been three missions to fly by Saturn and one to orbit the planet. In each case, radio occultation experiments (ROX) were conducted to observe plasma densities within Saturn's ionosphere. The fly-by occultations were acquired in 1979 by Pioneer 11 with both ingress and egress measurements, by Voyager 1 (with ingress only) in 1980, and then both ingress and egress measurements by Voyager 2 in 1981. These five initial N_e(h) profiles (summarized in Atreya et al., 1984) somewhat startled the science community studying outer planet ionospheres — both by their low magnitudes, and even more so by their variability. For our purposes, they yielded a total of five data points under high solar flux conditions for S2-layer maximum electron density (NmS2) and total electron content (TEC), with specific dates, local times, solar zenith angles, solar fluxes and latitudes. Starting in 2005, a new and much anticipated flow of ROX profiles came from the Cassini Mission to Saturn. These resulted in 59 additional N_e(h) profiles from which the same set of parameters were obtained (Kliore et al., 2014). Table 1 summarizes the dates of all 64 ROX measurements, together with the "rotated sun dates" as described above.

Vertical ionospheric electron density profiles at the giant planets are significantly more structured than at the terrestrial planets for currently unknown reasons. It is not always straightforward to identify a "main" ionospheric region at Saturn (the S2-layer). For consistency we always use the maximum electron density from each radio occultation profile as the representative value of NmS2, regardless of its altitude.

Following the methods described above for organizing observations of the martian ionosphere, the N_e(h) profiles from Saturn were adjusted in identical ways—thereby enabling their comparisons with Earth's ionosphere. These transformations lead to equivalent values for maximum electron density (NmS2) and TEC at Saturn's average orbital distance (9.582 AU) as follows:

(1) Under PCE conditions, NmS2 and TEC are inversely proportional to distance from the Sun and thus the correction of an observation from Saturn's elliptical orbit to its mean circular orbit is carried out by

$$NmS2(9.582\ AU) = NmS2(d_{Sat}) * \frac{d_{Sat}}{9.582\ AU} \tag{3}$$

where d_{Sat} is Saturn's distance from the Sun in AU. The same correction is made for TEC. At Saturn's relatively large distance from the Sun the magnitudes of such adjustments are rather small (typically a few percent).

(2) The solar proxy $F_{10.7}$ is similarly corrected to Saturn's average orbital distance from observations made at 1 AU:

$$F_{10.7}(9.582\ AU) = \left[F_{10.7}(1\ AU) * \left(\frac{1}{9.582\ AU} \right)^2 \right] \tag{4}$$

(3) The final adjustment needed for analyses to be conducted below is to take into account the fact that ionospheres at Earth and Mars do not change as dramatically on a day-to-day basis as the Sun's $F_{10.7}$ radio flux can (Richards et al., 1994; Mendillo et al., 2013). To account for this "sluggish" effect, Richards et al. (1994) introduced the practice to have a daily value of $F_{10.7}$ weighted equally with the three solar rotation (81-day) average centered on that day.

$$F_{eff} = \frac{F_{10.7} + \langle F_{10.7} \rangle_{81-day}}{2} \tag{5}$$

We assume the same relatively slow response at Saturn and continue to use Eq. (5).

3.2. Ionospheric morphology and variability at Saturn

The database for analysis resulting from the above methodology is depicted in Fig. 2. For each panel, data are displayed on the left showing 64 distinct data points. Each panel is then summarized

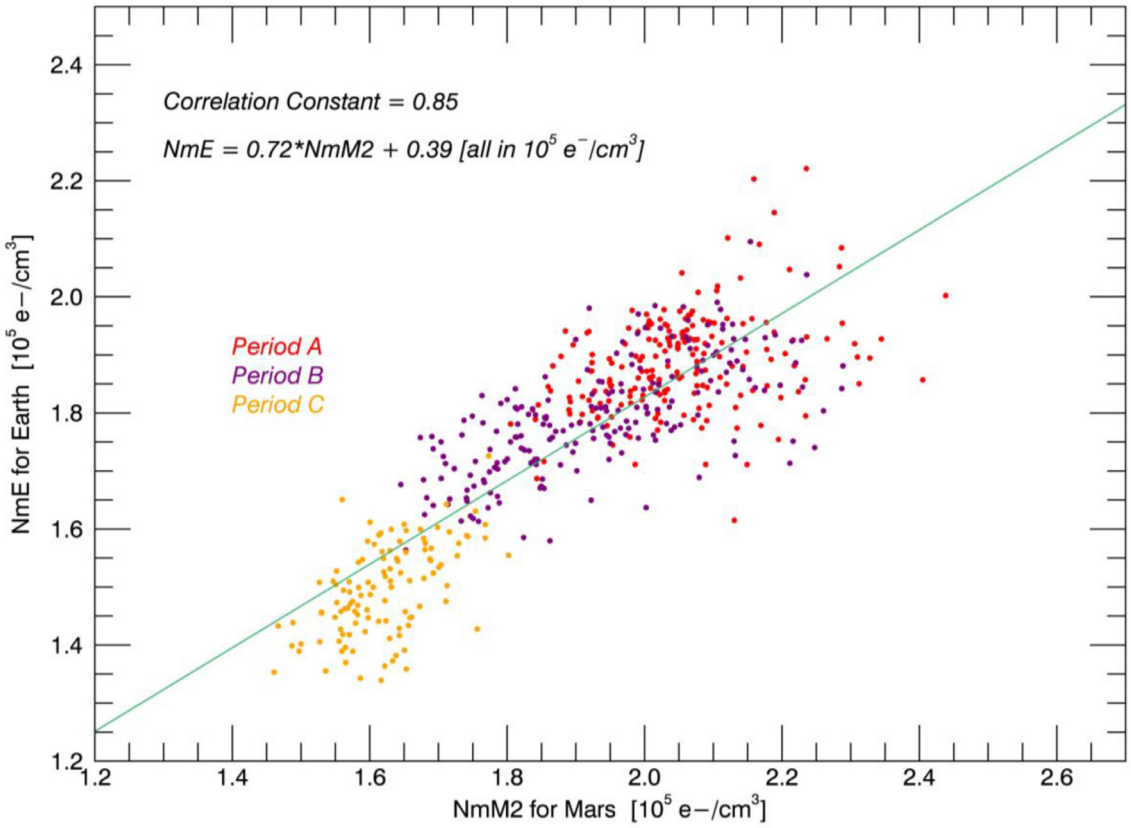

Fig. 1. Correlation of average daily sub-solar point values of NmE at Earth (1 AU) and NmM2 at Mars (1.524 AU) over the period 1 November 2001 to 9 June 2005. Periods A, B and C are characterized by the mean solar radio flux index at 1 AU being 170, 130 and 100 units (after Fig. 3 in Mendillo et al., 2016).

Table 1
Observation dates and Rotated-Sun-Dates for the Saturn ionosphere.

Date of measurement			Rotated Sun date (Earth)			Date of measurement			Rotated Sun date (Earth)		
D	M	Y	D	M	Y	D	M	Y	D	M	Y
1	9	1979	14	9	1979	16	6	2008	24	6	2008
1	9	1979	14	9	1979	16	6	2008	24	6	2008
12	11	1980	2	11	1980	23	6	2008	1	7	2008
26	8	1981	6	9	1981	7	7	2008	16	7	2008
26	8	1981	6	9	1981	7	7	2008	16	7	2008
3	5	2005	11	5	2005	1	11	2009	22	10	2009
3	5	2005	11	5	2005	1	11	2009	22	10	2009
21	5	2005	30	5	2005	20	11	2009	11	11	2009
21	5	2005	30	5	2005	9	12	2009	1	12	2009
8	6	2005	18	6	2005	9	12	2009	1	12	2009
26	6	2005	8	7	2005	26	12	2009	20	12	2009
26	6	2005	8	7	2005	26	1	2010	22	1	2010
15	7	2005	28	7	2005	26	1	2010	22	1	2010
2	8	2005	20	7	2005	27	4	2010	30	4	2010
2	8	2005	20	7	2005	27	4	2010	30	4	2010
20	8	2005	8	8	2005	18	6	2010	25	6	2010
5	9	2005	26	8	2005	18	6	2010	25	6	2010
17	9	2006	6	9	2006	24	7	2010	2	8	2010
10	5	2007	16	5	2007	2	9	2010	13	9	2010
10	5	2007	16	5	2007	1	8	2011	9	8	2011
11	6	2007	20	6	2007	1	8	2011	9	8	2011
28	6	2007	8	7	2007	5	6	2012	9	6	2012
24	10	2007	15	10	2007	12	8	2012	20	8	2012
24	10	2007	15	10	2007	12	8	2012	20	8	2012
19	12	2007	14	12	2007	2	9	2012	12	9	2012
19	12	2007	14	12	2007	5	1	2013	28	12	2012
15	1	2008	12	1	2008	31	1	2013	25	1	2013
8	2	2008	7	2	2008	25	2	2013	21	2	2013
17	5	2008	23	5	2008	10	5	2013	11	5	2013
17	5	2008	23	5	2008	20	5	2013	22	5	2013
1	6	2008	8	6	2008	31	5	2013	2	6	2013
1	6	2008	8	6	2008	31	5	2013	2	6	2013

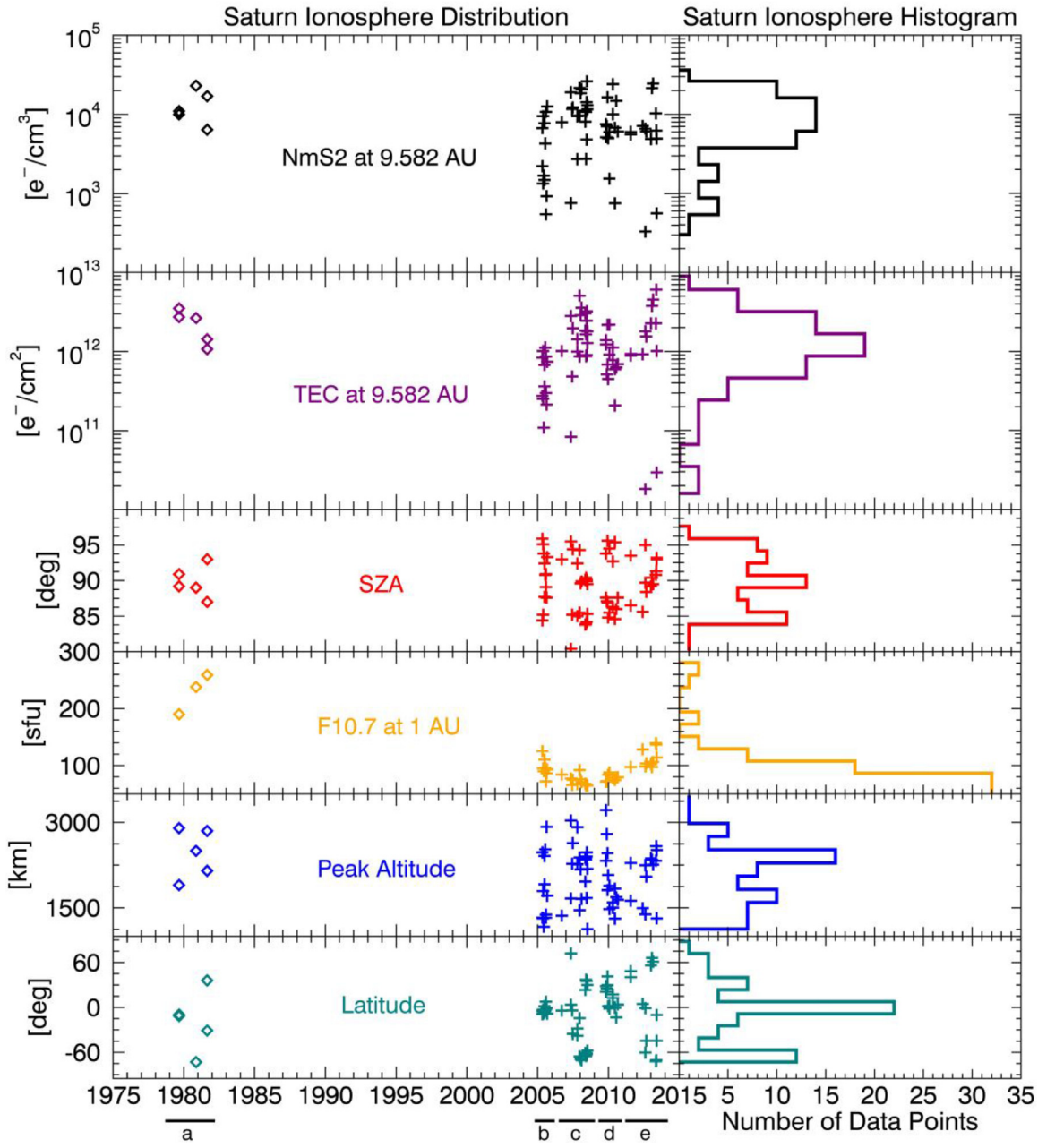

Fig. 2. Distribution of the 64 Saturn ionosphere data points in time (left) and their occurrence distributions (right). In the top panel, maximum electron densities (NmS2) are shown. Note that five of these data point come from the Pioneer-Voyager epoch (open diamonds) and the others are from Cassini observations (crosses). Two of non-Cassini peak density values have approximately the same value over-plotted at 10^4 e^-/cm^3. The remaining panels show total electron content values, solar zenith angles, solar cycle conditions shown by the solar radio flux (F10.7) at 1 AU, the altitudes of the NmS2 values, and the latitudes of the observations. Below the graphs, five epochs are indicated by (a) through (e) that summarize the Pioneer-Voyager period versus four "occultation seasons" during the Cassini era. These are treated in analyses described later in the paper.

using its histogram distribution on the right. There are several key points to notice in the panels, top to bottom, that describe parameters observed versus time spanning nearly 40 years.

- The peak electron density and TEC values from the Pioneer/Voyager era occurred during solar maximum years (1979–1981). Their high values are roughly in the same domain of high magnitudes found during Cassini's era of reduced solar flux values. This in itself suggests that variability in Saturn's ionosphere is not as dependent on solar irradiance as found in the inner solar system.
- Solar Zenith Angles (SZA) values are all greater than 80° and 29 data points are greater than 90°. This is due to the geometry of the Sun-Saturn-Earth system, which limits spacecraft-to-Earth occultation observations to the planet's solar terminator.
- In the $F_{10.7}$ panel, three points (versus 5) appear because each of the two Voyager ROX experiments occurred on the same calendar day. All solar maximum results thus come from these points only. All Cassini era data are for lower solar flux conditions.
- The altitudes of peak electron density found during solar maximum years are not particularly different from those found during lower solar flux years. In our analyses below, we will not dwell on altitude issues.

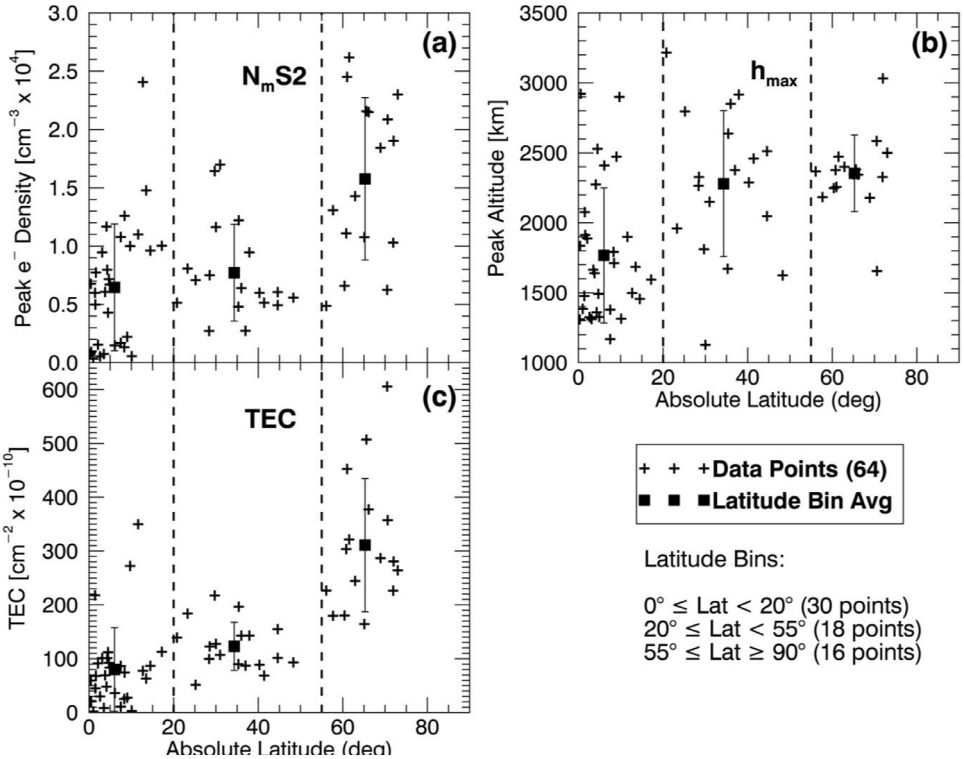

Fig. 3. Variations in Saturn's ionosphere as characterized by (a) the observed absolute magnitudes of maximum electron density (NmS2), (b) the altitudes of maximum density (h_{max}), and (c) total electron content (TEC). The data have been split into three latitude bins (after Kliore et al., 2014), separated by dashed lines. The statistical mean within each latitude regime is indicated by a square with 1-sigma standard deviations shown.

- The planetographic latitudes sampled during solar maximum years are also not significantly different from those found during the Cassini era.
- Below the time axis, periods of "occultation clusters" ('a' through 'e') refer to the Pioneer/Voyager era (a), and four "ROX seasons" of Cassini data (b) to (e). There are no obvious differences between these data clusters other than solar flux values.

3.3. Characterization of variability

In an attempt to find latitude patterns from the limited set of Cassini's radio occultation experiments, Kliore et al. (2014) introduced a format of portraying $N_e(h)$ parameters versus absolute values of latitude, rather than separate hemisphere distributions. We adopt the same approach and show in Fig. 3 the 64 values of maximum electron density (NmS2), height of maximum density (h_{max}), and TEC within three latitude domains: 0°—20°, 20° – 55°, and 55°—90°. The trans-equatorial-latitude results show the lowest average values for NmS2, h_{max} and TEC. The largest average values appear in the highest latitude range. These patterns for magnitudes of peak electron density and TEC are dominated by the 59 values from Cassini and summarize a trend noted earlier (Nagy et al., 2006, 2009; Kliore et al., 2009)—namely, a noticeable departure from the anticipated morphology that sub-solar conditions would exhibit the most robust ionosphere. The proposed resolution of this low-latitude anomaly came from modeling: the introduction of enhanced chemical loss rates due to an influx of water from the rings and icy moons (Moses and Bass, 2000; Moore et al., 2010). Here we do not concentrate on the issue of NmS2 magnitudes, but rather on the variability about average behavior, a topic explored in neither statistical nor modelling studies to date.

Table 2 summarizes the numerical results depicted in Fig. 3. The patterns of central interest are the standard deviation (one-sigma) variability values computed in percent with respect to the mean values for peak density and TEC in each latitude region. Given the small values of peak density and TEC at low latitudes, their standard deviations in percent are larger (84% and 97%) than those computed at mid-latitudes (54% and 36%) and high-latitudes (44% and 40%).

The high $\sigma(\%)$ values for Saturn's ionosphere are significantly larger than the typical < 10% variability values found for the molecular ion layers at Earth and Mars (and also for the ~20–25% values for the atomic ion F2-layer at Earth). Such numbers suggest that mechanisms other than basic PCE are the dominant ionospheric formation and control processes at Saturn. To show this quantitatively, we will form NmS2 and TEC patterns versus solar flux, and then apply to Saturn the analysis methods for "same-solar-flux" comparisons described above for Earth and Mars.

3.4. Comparisons with PCE parameters

As shown in previous studies of photochemical equilibrium (PCE) conditions, electron densities depend on the ionizing solar radiation as well as the solar zenith angle. Using Eqs. (3), (4) and (5), correlations at 9.582 AU should be as

$$NmS2 \text{ or } TEC \propto \sqrt{F_{eff} * \cos(SZA)} \quad (6)$$

The Saturn radio occultation experiments all occur close to (or beyond) the solar terminators at dawn and dusk. With SZA > 90°, use of cos(SZA) becomes non-physical. Moreover, 56 of the 64 total points have SZA greater than 85°. Rather than delete the 29 values with SZA > 90° and use those between 85° and 90°, we simply set SZA = 85° for all cases of SZA > 85°. The results are shown in Fig. 4, with the 29 values for SZA > 90° converted to 85° shown in red. Notice that this adjustment affects all three data sources—Pioneer and Voyager (diamonds) and Cassini data (crosses).

The results in Fig. 4 are far from an impressive display of PCE conditions. As anticipated from Fig. 2, the five pre-Cassini

Table 2
Latitude bin averages and their standard deviations [σ(%)] for maximum electron density (NmS2), total electron content (TEC) and peak altitude (h_{max}), as illustrated in Fig. 3.

Latitude Bin ⟨average⟩ (# of obs)	NmS2 (e^-/cm^3)	stddev (e^-/cm^3)	% of % of avg	TEC (10^{10} e^-/cm^2)	stddev (10^{10} e^-/cm^2)	% of avg	h_{max} (km)	stddev (km)	% of avg
low ⟨6.0°⟩ (30 pts)	6461	5441	84.2	80	77.6	97.1	1767	482	27.3
mid ⟨34.3°⟩ (18 pts)	7720	4151	53.8	123	44.6	36.3	2280	521	22.9
high ⟨65.3°⟩ (16 pts)	15,771	6962	44.1	311	124.0	39.8	2353	273	11.6

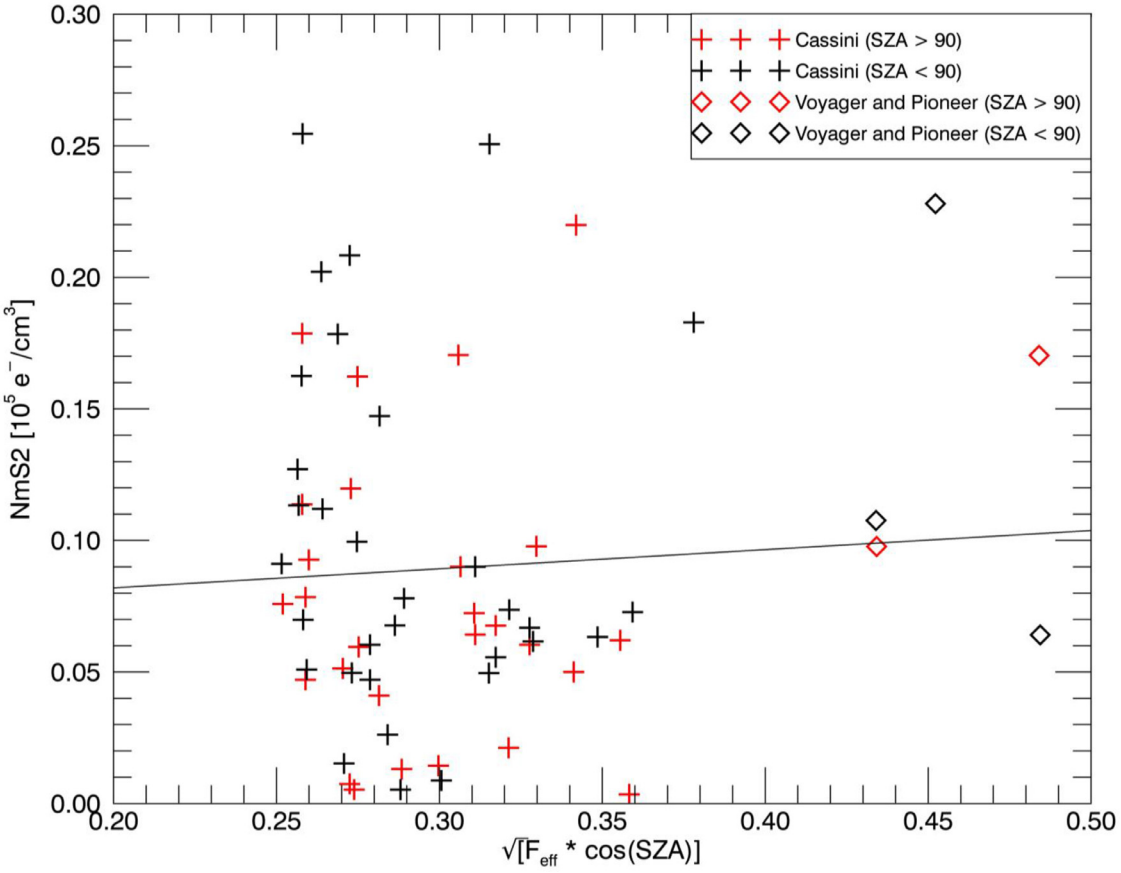

Fig. 4. Saturn ionosphere correlation between peak electron density (N_mS2), solar flux proxy (F_{eff}), and SZA at the mean orbital distance of 9.582 AU. The linear correlation coefficient is 0.06, with the line shown is NmS2 = 0.07 $\sqrt{(F_{eff} * \cos(SZA))} + 0.07$ [units = 10^5 e^-/cm^3]. The cutoff at 0.25 units along the horizontal axis results from setting SZA > 85° to 85°.

data points determine the totality of solar maximum samples, and their average provides the mild slope and weak correlation shown. Omitting the pre-Cassini points results in a correlation coefficient of −0.19. To search for optimal correlations, we conducted several studies using sub-sets of data (e.g., latitude bins, dawn versus dusk). No improvement in linear correlation coefficient occurred for any method tried at low latitudes, but a positive trend was found for middle and high latitudes. These are shown in Fig. 5, with linear correlations coefficients of 0.50 for peak density and 0.35 for TEC. These results assert a modest conformity of Saturn's ionosphere with PCE conditions at latitudes where influxes of water do not dominate the recombination chemistry (Moore et al., 2006a; 2010).

3.5. Comparison with Earth

Encouraged by the results of the "same-solar-condition-days" analyses conducted between Earth and Mars (shown in Fig. 1), we attempted the same approach for Saturn. With far fewer data points at Saturn, the situation is made even worse due to the fact that radio occultation experiments have both ingress and egress

Table 3
Terrestrial ionosonde sites providing data on the 43 common days of ROX observations at Saturn.

Station	Latitude (°N)	Longitude (°E)	Missing days
Boulder	40.02	-105.27	3
Brisbane	-27.53	152.92	10
Grahamstown	-33.31	26.53	11
Point Arguello	34.58	-120.65	20
Wallops Island	37.88	-75.44	9

experiments on the same calendar day (whether a fly-by mission or by Cassini in orbit). This results in the 64 measurements used above (see Table 1) to be reduced to 43 days of observations. For each of these 43 days, measurements at Earth on the "rotated sun date" are needed. To do so, we selected five ionosonde stations at mid-latitudes from both hemispheres (see Table 3) that have good reporting rates for daily observations. To assess the E-layer patterns under optimal conditions, we conducted our initial analysis using mid-day observations (to be shown in Figs. 6 and 7, below). Then, for comparisons with Saturn's radio occultation data

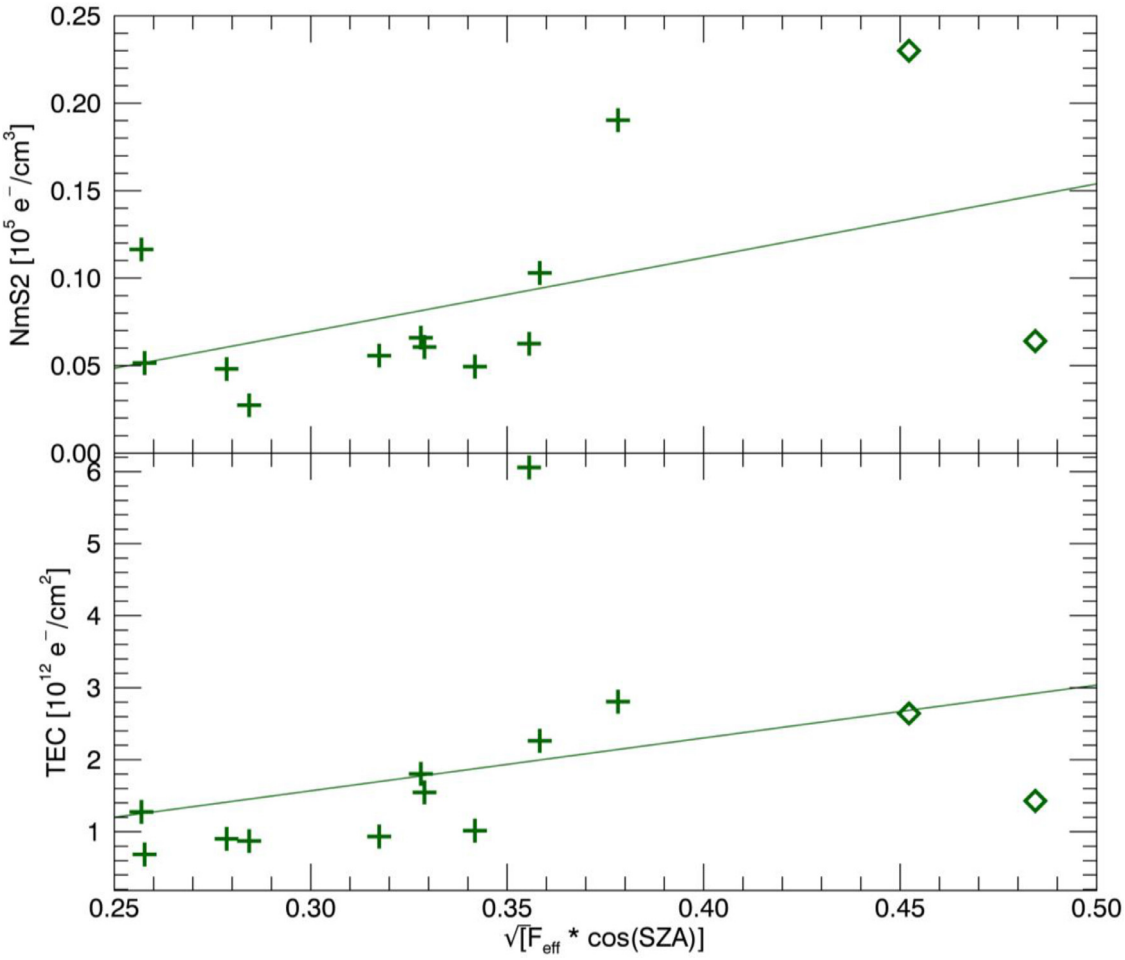

Fig. 5. Saturn's peak electron density (NmS2) and TEC versus PCE parameter (Eq. (6)) for observations at dusk and at mid/high latitudes (20°–90°). The best fit linear equations and their correlation coefficients (CC) are: NmS2 = 0.42 $\sqrt{(F_{eff} * \cos(SZA))} + 0.06$ [units = 10^5 e^-/cm^3], CC = 0.50; TEC = 7.39 $\sqrt{(F_{eff} * \cos(SZA))} + 0.04$ [units = 10^{12} e^-/cm^3], CC = 0.35.

(Fig. 8), we used E-layer observations made close to solar termination times.

For our initial E-layer analysis, we selected the three hourly observations spanning mid-day (11:00–13:00 local time) for the reflection frequencies of the E-layer (f_oE), converted them to plasma densities, and computed one "mid-day average" ($<NmE>$) for each station. Instrument problems did result in some missing days at several stations, and thus the total number of possible mid-day values (5 stations x 43 days = 215 station-days) was reduced to a total number of 162 data points (see Table 3). To compare these with observations at Saturn, we first used the terrestrial versions of Eqs. (3, 4 and 5) to arrive at values at 1AU. This comparison of ⟨NmE⟩ with PCE drivers is shown in Fig. 6.

The results shown in Fig. 6 reveal that the magnitudes of peak electron densities in the E-layer ($1–2 \times 10^5$ e^-/cm^3) at mid-day are somewhat larger than an order of magnitude different from the global near-terminator average ($<NmS2> = \sim 1 \times 10^4$ e^-/cm^3) of Saturn's S2 layer (see top panel of Fig. 2). This is approximately the expectation from PCE theory if a molecular ion ionosphere were moved from 9.582 AU to 1AU (i.e., by the *1/d* correction shown in Eq. (3)) and the local times adjusted by solar zenith angles. This validates, in the most general way, that the global ionosphere at Saturn has peak electron densities governed by basic solar production and chemical loss.

The low correlation (0.32) of the terrestrial E-layer with its PCE drivers, as shown in Fig. 6, is an unanticipated finding. The solar flux values used in this analysis come from the very strong solar maximum years of 1979–1981 and the weak solar cycle periods of 2005–2013 (see Fig. 2). Changes in the neutral atmosphere also occur over solar cycle time spans, and these include thermal expansion/contraction and changes due to waves and tides. Yet, the PCE Eq. (6) only takes into consideration solar photon drivers. Given that day-to-day variability is present in any ionosphere, spot comparisons of data points spanning decades might well lead to spurious results.

To explore PCE trends over the longest time span of observations of Saturn's ionosphere, we use the "radio occultation epochs" indicated by the letters 'a' through 'e' at the bottom of Fig. 2. We averaged the data at Saturn during each epoch resulting in a total of five data points for NmS2 and TEC. These results are shown in Fig. 7(a, b). Clearly, it is difficult to suggest that a trend appears in the Cassini era observation—the correlations of 0.50 and 0.53 coming entirely from the single Pioneer/Voyager era data point. For the five ionosonde stations at Earth, however, the same five epochs yielded a total of twenty-two (out of a possible twenty-five) ⟨NmE⟩ values (i.e., due to data losses noted in Table 3). Their correlation with the PCE driver parameter is given in Fig. 7(c). The much higher correlation coefficient (0.84) from such broad temporal averaging methods points to the anticipated long-term consistency of the terrestrial E-layer with its solar PCE drivers. Note, in particular, that all five data points for the Pioneer/Voyager epoch are clearly above those from the Cassini era.

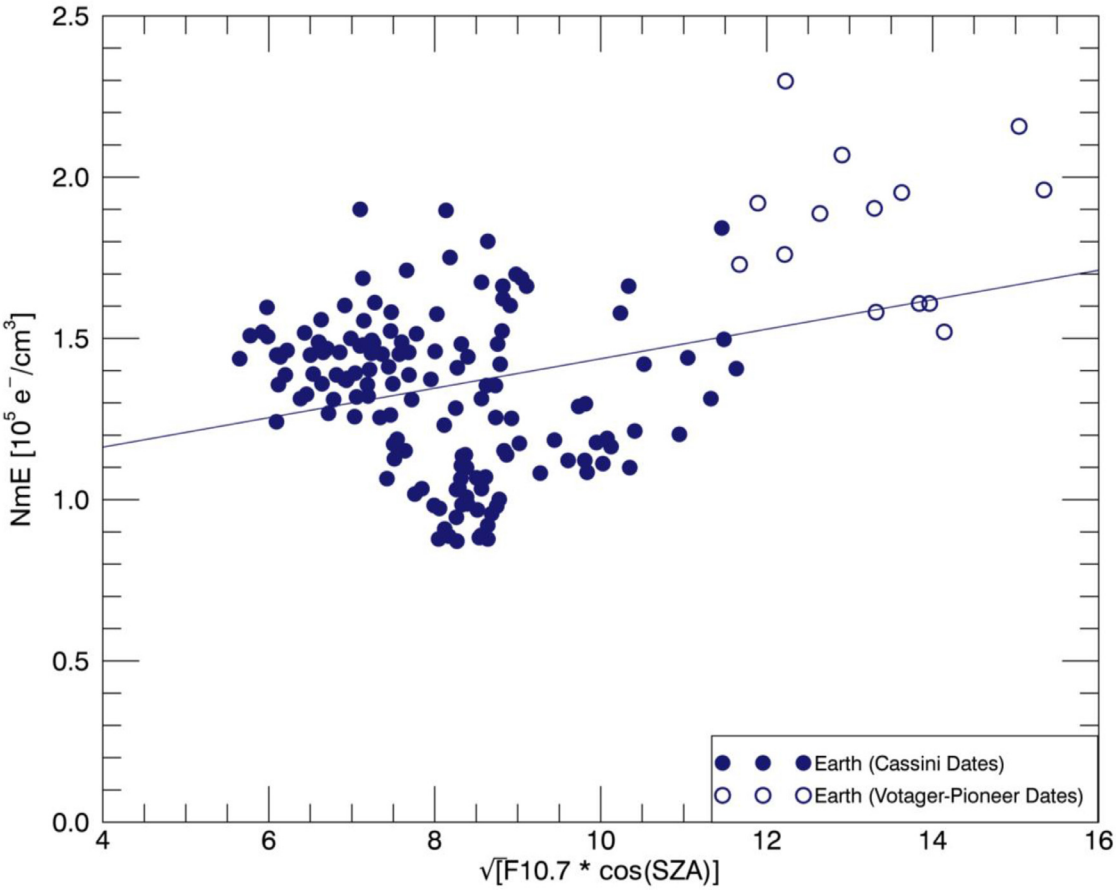

Fig. 6. Observations from five ionosonde stations at Earth for mid-day average values of NmE correlated with the PCE parameter (Eq. (6)). The best-fit linear relationship is NmE = 0.05 $\sqrt{(F_{eff} * \cos(SZA))} + 0.98$ [units = 10^5 e^-/cm^3], CC = 0.32.

Our ultimate analysis goal—to obtain the Saturn–Earth version of Fig. 1 for same-solar-condition-days at two planets—can now be conducted. The protocol adopted uses the rotated-sun method to identify the dates to compare, makes the *1/d* corrections to form values for equivalent circular orbits (1.0 and 9.582 AU), and selects fixed solar zenith angles to use (e.g., the SZA = 0° points were used in Fig. 1). For the Earth-Saturn pair, all of the Saturn observations were made very close to solar terminator conditions, and thus for the Earth's ionosonde data we selected the hourly value closest to SZA = 85° to provide comparable conditions. The results for Saturn's NmS2 and Earth's ⟨NmE⟩ are shown in Fig. 8. Obviously, given the poor correlations between Saturn's ionosphere and its solar drivers explored in considerable detail above, the resultant Earth-Saturn correlations were not expected to be high. As Fig. 8 shows, they actually have an anti-correlation (with a low correlation coefficient of CC = −0.19). A separate analysis with data converted to sub-solar conditions (SZA = 0°) yielded no change to this. Finally, recalling from Fig. 5 that the highest correlation between PCE drivers and Saturn's peak electron density and TEC data came from observations at middle and high latitudes in the dusk sector, we found the correlation between NmE and NmS2 data for those conditions to be only 0.29—far from an impressive optimization.

4. Modeling

The analyses of observations described above all pointed to the fact that Saturn's ionosphere is a highly variable plasma with fluctuations in peak density and TEC that far exceed those found at Earth and Mars. These changes cannot be due to variability in solar irradiance. Given that the S2-layer is embedded within a dense thermosphere, PCE conditions must still dominate, and thus sources of variability must be due to externally-imposed fluctuations in chemistry or intrusions of dynamics to an extent not yet understood. Here we approach this problem as a function of latitude.

4.1. Source of variability at low latitudes: models of changing water flux

Dating back to the original Pioneer 11 and Voyager measurements, models of Saturn's ionosphere have invoked an external influx of oxygenated particles in order to reduce modeled electron densities and thereby more accurately reproduce NmS2 (e.g., Connerney and Waite, 1984). In order to simplify terminology, this influx of external material is typically collectively referred to as a "water flux", though it may not come in as purely H_2O. A water flux quenches Saturn's ionosphere by converting long-lived H^+ ions into short-lived molecular ions, which quickly dissociatively recombine with electrons thereby reducing the net plasma density. Using the one-dimensional version of the Saturn-Thermosphere-Ionosphere-Model (STIM), Moore et al. (2006a) demonstrated that a water flux still provided the best match to early Cassini radio occultation observations. Further modeling of the effects of variable influxes of water on Saturn's ionosphere was presented in Moore and Mendillo (2007) and Moore et al. (2010).

The water influx at Saturn is thought to be mostly due to a combination of two processes: a neutral source of water products from the active cryovolcanic moon, Enceladus, and an ionized source of charged oxygen particles from Saturn's rings called

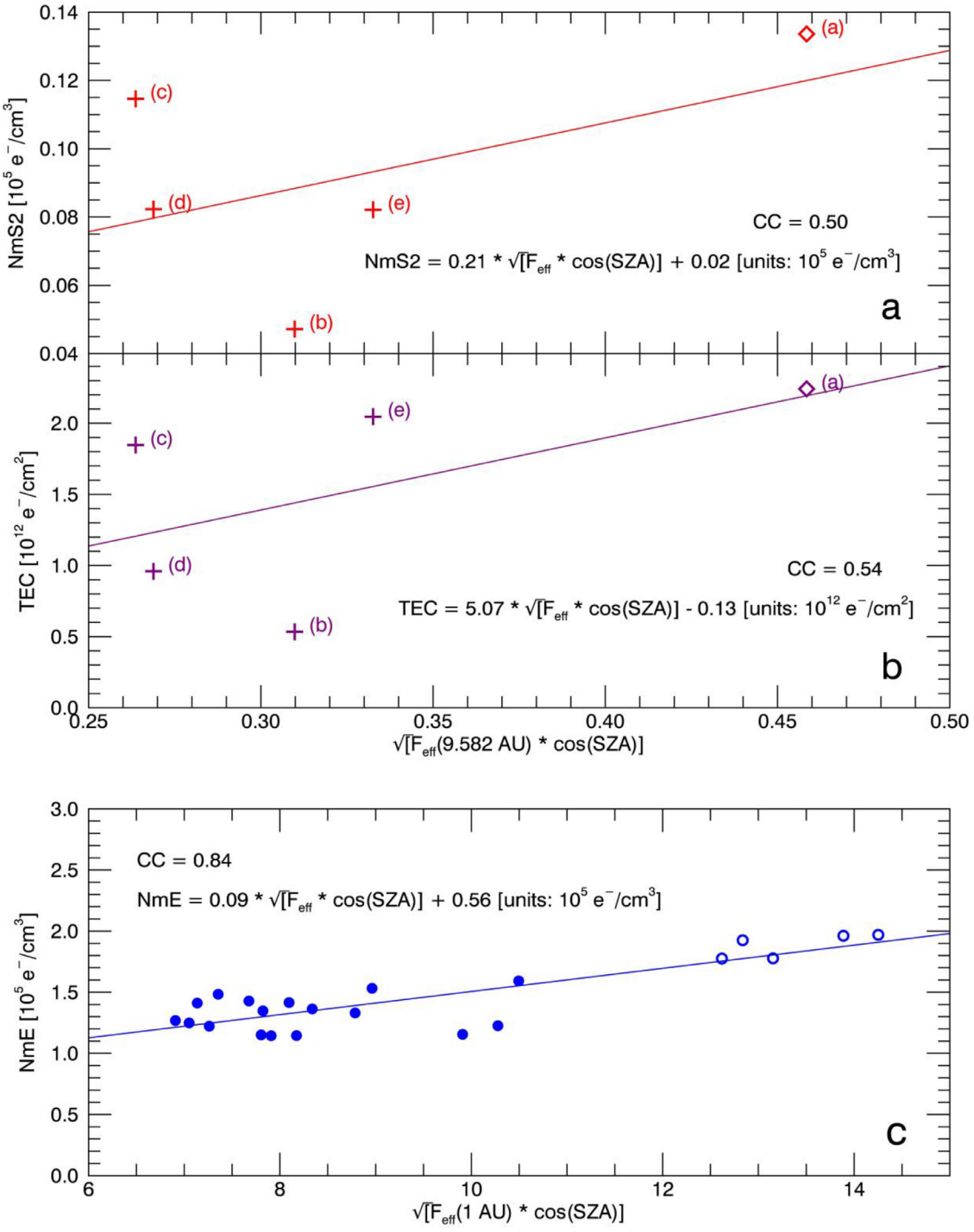

Fig. 7. Correlation of solar PCE parameters with average ionospheric parameters at Saturn's mean orbital distance (9.582 AU) and at Earth (1 AU) for the five radio occultation epochs at Saturn indicated in Fig. 2. Panel (a) gives Saturn peak electron density average values, panel (b) gives TEC average values, and panel (c) gives epoch averages for <NmE> from ionosonde stations at Earth.

"ring rain" (e.g., Connerney, 1986; Prangé et al., 2006). The neutral source is predicted to be smoothly varying with latitude, with a peak influx at the equator (Jurac and Richardson, 2007; Cassidy and Johnson, 2010; Hartogh et al., 2011; Fleshman et al., 2012), whereas ring rain is expected to vary strongly with latitude, depending on the region of Saturn's rings magnetically linked to the ionosphere. The strongest ring rain source of water is thought to originate from the inner edge of Saturn's B ring (near 37S and 43 N planetocentric latitude; Northrop and Connerney, 1987; Ip, 1984; (O' Donoghue et al., 2013; 2017), though it is possible that some positively-charged dust grains may precipitate near Saturn's equator as well (e.g., Ip et al., 2016).

It is reasonable to expect that there would be temporal as well as spatial variations of water influx. For example, the Enceladus plume neutral water source rate is variable by up to an order of magnitude (Smith et al., 2010), and is correlated with tidal stresses (Hedman et al., 2013; Ingersoll and Ewald, 2017), though how this variability is translated into changing water fluxes in Saturn's at-

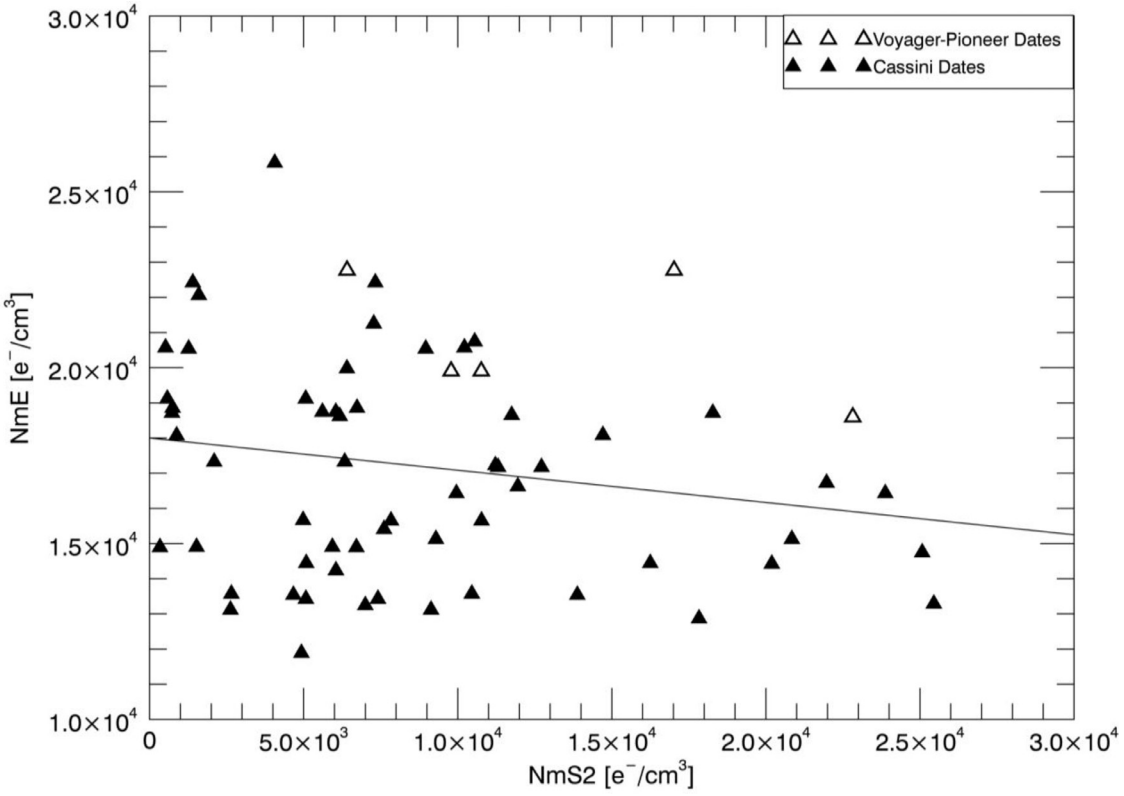

Fig. 8. NmE vs NmS2 for SZA = 85°. With each of the ROX profiles at Saturn having the same calendar date for ingress and egress, we double-counted the terrestrial E-layer data for that date. The equation of the best fit linear correlation is NmE = −0.09*NmS2 + 1.8 [units = 10^4 e^-/cm^3], with a correlation coefficient (CC) = −0.19.

mosphere is not clear. An additional complication comes from currently unconstrained ionospheric chemistry: H^+ can also be efficiently removed from the ionosphere via charge exchange with H_2, but only if H_2 is in the 4th or higher vibrational state. At present there are no firm constraints on the H_2 vibrational populations in Saturn's upper atmosphere.

From Table 2, the variability of the NmS2 value in Saturn's low-latitude ionosphere is described by the standard deviation σ (1 sigma) value of ± 5441 e^-/cm^3, corresponding to ± 84% about the sample mean. [The mean value itself (6461 e^-/cm^3) has an error-of-the mean of ~15%, computed from $\sigma/\sqrt{n}$, where n = number of observations.] From the model calculations of Moore et al. (2015), this NmS2 average electron density corresponds to a water flux of $\sim 4 \times 10^6$ cm^{-2} s^{-1}. Variability of ~ 84% about the mean NmS2 could be explained by a range of water flux from roughly (2 – 50) x 10^6 cm^{-2} s^{-1}. Fig. 9 shows model results demonstrating this range of NmS2 magnitudes resulting from such a range of water influx values. This leads us to conclude that if the rate of low-latitude water influx varies by a factor of ~25, either in time or in latitude, then it alone can provide an adequate explanation for the large degree of variability observed in Saturn's low-latitude ionosphere.

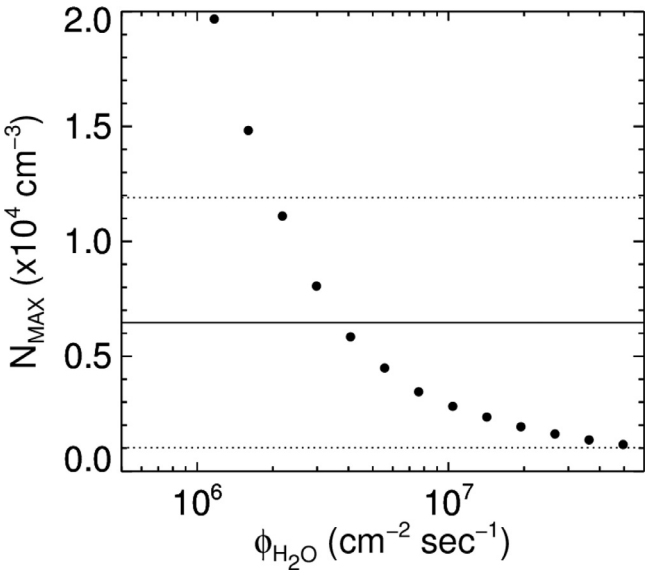

Fig. 9. Simulation results for maximum electron density at Saturn (NmS2) as a function of water influx at low latitudes (± 20°). The mean low-latitude NmS2 from spacecraft radio occultations is given by the solid black line, while dotted black lines indicate the full range of variability about the mean. Filled circles are taken from model runs used to create Fig. 5 of Moore et al. (2015).

4.2. Sources of variability at high latitudes: models of changing auroral input

Previous simulations using the general circulation model (GCM) version of the Saturn Thermosphere Ionosphere Model (STIM) investigated effects of auroral input upon Saturn's high latitude thermosphere and ionosphere (Mueller-Wodarg et al.,2012). To examine the impact of short-term variability in the magnetosphere upon the high latitude ionosphere, the auroral influx of 10 keV electrons was "pulsed" to twice its regular value for the duration of 1 Saturn hour (1/24th of the Saturn rotation period = 26 minutes). The result was an immediate increase (up to 60%) in local peak electron density due to local electron impact ionization. As a result, local Joule heating caused a local thermosphere temperature increase and local upwelling in the thermosphere, similar to that seen on Earth at high latitudes (Rishbeth and Mueller-Wodarg, 1999).

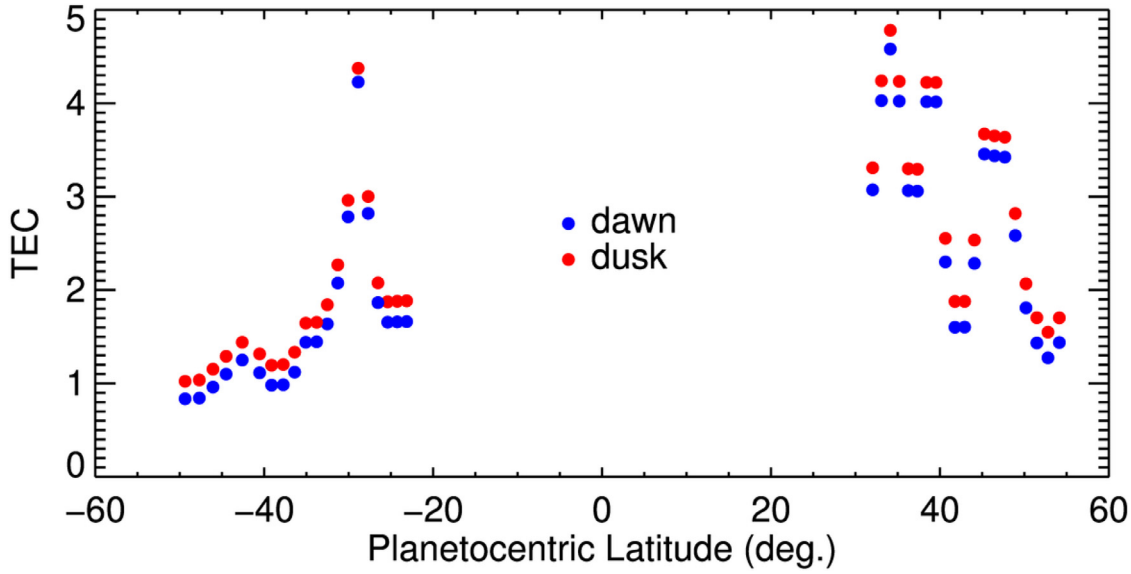

Fig. 10. Simulation of latitude structure for TEC at Saturn. The latitudinal variations are driven by variations in estimated water influx from Saturn's rings (Moore et al., 2015), based on ground-based observations of ionospheric H_3^+ emissions (O'Donoghue et al., 2013).

The change in Saturn's thermosphere involved a reduction in local H abundances by 5–10%. The effect of this neutral composition change on the ionosphere was found to be negligible on the time scale of short term (day-to-day) variability. Thus, except for latitudes precisely below regions of strong energetic particle precipitation, the variations in Saturn's high latitude ionosphere shown in Fig. 3 remain unexplained. That is, it is unlikely that each radio occultation observation at high latitudes occurred above an auroral event. Auroral morphologies at Saturn have been studied using HST (e.g., Clarke et al., 2005; Nichols et al., 2009), ground-based telescopes (Stallard et al., 2008a), and Cassini (Stallard et al., 2008b; Melin et al., 2011). While considerable variations occur from the equatorward edge of the auroral oval to across the polar cap, there are no dramatic cases of equatorward excursions of auroral storms—as often seen on Earth.

4.3. Sources of variability at middle latitudes: intrusions of low-latitude and high-latitude sources of variability into mid-latitudes

While most model calculations have used a fixed latitude distribution of water influx at low latitudes—with only the flux magnitudes varying—the latitude distribution of water influx itself could vary. This would introduce episodes of enhanced loss into the mid-latitude ionosphere. Moreover, with mid-latitudes subjected to "ring rain" processes as an additional (and variable) source or perturbation, ample mechanisms would seem to exist to account for the mid-latitude variations depicted in Fig. 3.

A demonstration of the ring rain effect is given in Fig. 10, which shows modeled TEC versus latitude based on the water fluxes derived in Fig. 8 of Moore et al. (2015). Moore et al. (2015) estimated that, based on ground-based observations of H_3^+ ring rain signatures, the ring-derived water flux could vary by more than an order of magnitude over only a few degrees of latitude. The strong variations in TEC are matched by similar variations in NmS2, and they are driven primarily by the ring-derived water influxes estimated from model comparisons with the latitudinal variations of H_3^+ emissions (O' Donoghue et al., 2013; 2017). Note that the Moore et al. (2015) simulations were performed for comparisons with a specific day of H_3^+ observations (17 April 2011), and therefore cannot be compared directly with the variations in electron density derived from the radio occultations summarized in Fig. 3 which were obtained over a wide range of seasonal and solar conditions. Nevertheless, Fig. 10 illustrates that we can expect a significant mid-latitude variability in electron density based solely on estimates of ring-derived water influx.

Thus, even if the Enceladus source of water influx occurred only at low latitudes, and auroral input was confined to high latitudes, the ring-rain source at middle latitudes could account for the observed variations in Saturn's ionospheric peak electron density and total electron content.

5. Summary and conclusions

We have conducted the first quantitative study of variations in Saturn's ionosphere using all of the radio occultation experiment (ROX) profiles available from four satellite missions (Pioneer-11, Voyager 1 and 2, and Cassini). The primary data product from a ROX experiment is the electron density profile, $N_e(h)$. As was amply documented in earlier studies of those profiles, the variations in maximum electron density (NmS2) and total electron content [TEC $= \int N_e(h)\, dh$] were surprisingly high. We have quantified this variability as a function of latitude and examined the main source of variability usually associated with ionospheres in photochemical equilibrium—changes in solar flux. Simulations using the Saturn Thermosphere-Ionosphere Model (STIM) were used to probe the role(s) of non-solar sources of variability. Our findings may be summarized as follows: (1) Saturn's ionosphere is clearly not dominated by solar flux to the degree found within the ionospheres of Earth and Mars; (2) some of the observed ionospheric variability at Saturn may be explained by spatial and/or temporal variations in "water" influx at low and middle latitudes; (3) ionospheric variability at high latitudes may be due to fluctuations in auroral input, but the spatial distribution of such effects is not included in current models; (4) while we used only the NmS2 and TEC parameters from ROX profiles, the degree of vertical $N_e(h)$ structure below the height of maximum density is likely an indication that significant additional variability may be driven by coupling between the ionosphere-thermosphere system and the deeper atmosphere below.

Acknowledgements

This work was support primarily by the NSF INSPIRE grant to Boston University for studies of comparative ionospheres (#1545–581), with additional support from research funds provided through the Center for Space Physics. MM acknowledges sabbatical support for collaborative research from Imperial College, London, during Fall 2016.

References

Cassidy, T.A., Johnson, R.E., 2010. Collisional spreading of Enceladus' neutral cloud. Icarus 209 (2), 696–703. doi:10.1016/j.icarus.2010.04.010.

Clarke, J.T., Gérard, J.-C., Grodent, D., Wannawichian, S., Gustin, J., Connerney, J., Crary, F., Dougherty, M., Kurth, W., Cowley, S.W.H., Bunce, E.J., Hill, T., Kim, J., 2005. Morphological differences between Saturn's ultraviolet aurorae and those of Earth and Jupiter. Nature 433 (7027), 717–719. doi:10.1038/nature03331.

Connerney, J., Waite, J., 1984. New model of Saturn's ionosphere with an influx of water from the rings. Nature 312, 136–138.

Connerney, J.E.P., 1986. Magnetic connection for Saturn's rings and atmosphere. Geophys. Res. Lett. 13 (8), 773–776.

Fleshman, B.L., Delamere, P.A., Bagenal, F., Cassidy, T., 2012. The roles of charge exchange and dissociation in spreading Saturn's neutral clouds. J. Geophys. Res. 117 (E5), E05007. doi:10.1029/2011JE003996.

Forbes, J., Palo, S., Zhang, X., 2000. Variability of the ionosphere. J. Atmos. Solar Terr. Phys. 62, 685–693.

Fox, M., Mendillo, M., Klobuchar, J., 1991. Ionospheric equivalent slab thickness and its modeling applications. Radio Sci. 26, 429–438. doi:10.1029/90RS02624.

Hartogh, P., Lellouch, E., Moreno, R., Bockelée-Morvan, D., Biver, N., Cassidy, T., Rengel, M., Jarchow, C., Cavalié, T., Crovisier, J., Helmich, F.P., Kidger, M., 2011. Direct detection of the Enceladus water torus with Herschel. Astron. Astrophys. 532 (L2). doi:10.1051/0004-6361/201117377.

Hedman, M.M., Gosmeyer, C.M., Nicholson, P.D., Sotin, C., Brown, R.H., Clark, R.N., Baines, K.H., Buratti, B.J., Showalter, M.R., 2013. An observed correlation between plume activity and tidal stresses on Enceladus. Nature 500 (7461), 182–184. doi:10.1038/nature12371.

Ingersoll, A.P., Ewald, S.P., 2017. Decadal timescale variability of the Enceladus plumes inferred from Cassini images. Icarus 282, 260–275. doi:10.1016/j.icarus.2016.09.018.

Ip, W.-H., 1984. On the equatorial confinement of thermal plasma generated in the vicinity of the rings of Saturn. J. Geophys. Res. 89 (A1), 395–398.

Ip, W.-H., Liu, C.-M., Pan, K.-C., 2016. Transport and electrodynamical coupling of nano-grains ejected from the Saturnian rings and their possible ionospheric signatures. Icarus 276, 163–169. doi:10.1016/j.icarus.2016.04.00.

Johansson, J., Buonsanto8, M., Klobuchar, J., 1978. The variability of ionospheric time delay. In: Goodman, J. (Ed.), Proceedings of the Symposium on the Effect of the Ionosphere on Space and Terrestrial Systems. Nav. Res. Lab., Washington, DC, pp. 1–7.

Jurac, S., Richardson, J.D., 2007. Neutral cloud interaction with Saturn's main rings. Geophys. Res. Lett. 34 (8), L08102. doi:10.1029/2007GL029567.

Kliore, A., Nagy, A., Asmar, S., Anabtawi, A., Barbinis, E., Fleischman, D., Kahan, D., Klose, J., 2014. The ionosphere of Saturn as observed by the Cassini Radio Science System. Geophys. Res. Lett. 41. doi:10.1002/2014GL060512.

Martinis, M., Wilson, J., Mendillo, M., 2003. Modeling day-to-day ionospheric variability on Mars. J. Geophys. Res. Space Phys. 108 (A10). doi:10.1029/2003JA009973.

Melin, H., Stallard, T., Miller, S., Gustin, J., Galand, M., Badman, S.V., Pryor, W.R., O'Donoghue, J., Brown, R.H., Baines, K.H., 2011. Simultaneous Cassini VIMS and UVIS observations of Saturn's southern aurora: comparing emissions from H, H 2 and H 3+at a high spatial resolution. Geophys. Res. Lett. 38 (15), 1–5. doi:10.1029/2011GL048457.

Mendillo, M., Marusiak, A., Withers, P., Morgan, D., Gurnett, D., 2013. A new semi-empirical model of the peak electron density of the Martian ionosphere. Geophys. Res. Lett. 40, 1–5. doi:10.1002/2013GL057631.

Mendillo, M., Trovato, J., Narvaez, C., Mayyasi, M., Moore, L., Vogt, M., Fallows, K., Withers, P., Martinis, C., 2016. J. Geophys. Res. Space Phys. 121. doi:10.1002/2016JA023097.

Mendillo, M., Smith, S., Wroten, J., Rishbeth, H., 2003. Simultaneous ionospheric variability on Earth and Mars. J. Geophys. Res. Space Phys. 108 (A12), 1432. doi:10.1029/2003JA009961.

Mendillo, M., Nagy, A., Waite, J.H. (Eds.), 2002. Atmospheres in the Solar System: Comparative Aeronomy (2002), Geophysical Monograph #130. American Geophys. Union, Washington, DC.

Moore, L., Mendillo, M., 2007. Are plasma depletions in Saturn's ionosphere a signature of time-dependent water input. Geophys. Res. Lett. 34 (12), L12202. doi:10.1029/2007GL029381.

Moore, L., Mendillo, M., Martinis, C., Bailey, S., 2006a. Day-to-day variability of the E layer. J. Geophys. Res. 111 (A6), A06307. doi:10.1029/2005JA011448.

Moore, L., Nagy, A.F., Kliore, A.J., Müller-Wodarg, I., Richardson, J.D., Mendillo, M., 2006b. Cassini radio occultations of Saturn's ionosphere: model comparisons using a constant water flux. Geophys. Res. Lett. 33 (22), L22202. doi:10.1029/2006GL027375.

Moore, L., Mueller-Wodarg, I., Galand, M., Kliore, A., Mendillo, M., 2010. Latitudinal variations in Saturn's ionosphere: Cassini measurements and model comparisons. J. Geophys. Res. 115 (A11), A11317. doi:10.1029/2010JA015692.

Moore, L., O'Donoghue, J., Müller-Wodarg, I., Galand, M., Mendillo, M., 2015. Saturn ring rain: model estimates of water influx into Saturn's atmosphere. Icarus 245, 355–366. doi:10.1016/j.icarus.2014.08.041.

Nagy, A., Balogh, A., Cravens, T., Mendillo, M., Müller-Wodarg, I., 2008. In: Comparative Aeronomy, 139. Springer Science+Business Media B. V, pp. 1–4. doi:10.1007/s11214-008-9353-0, Space Sci. Rev..

Nichols, J.D., Badman, S.V., Bunce, E.J., Clarke, J.T., Cowley, S.W.H., Crary, F.J., Dougherty, M.K., Gérard, J.-C., Grodent, D., Hansen, K.C., Kurth, W.S., Mitchell, D.G., Pryor, W.R., Stallard, T.S., Talboys, D.L., Wannawichian, S., 2009. Saturn's equinoctial auroras. Geophys. Res. Lett. 36 (24), L24102. doi:10.1029/2009GL041491.

Northrop, T.G., Connerney, J.E.P., 1987. A micrometeorite erosion model and the age of Saturn's rings. Icarus 70, 124–137.

O'Donoghue, J., Stallard, T.S., Melin, H., Jones, G.H., Cowley, S.W.H., Miller, S., Baines, K.H., Blake, J.S.D., 2013. The domination of Saturn's low-latitude ionosphere by ring "rain,". Nature 496 (7444), 193–195. doi:10.1038/nature12049.

O'Donoghue, J., Moore, L., Connerney, J.E.P., Melin, H., Stallard, T.S., Miller, S., Baines, K.H., 2017. *Re*-detection of the ionospheric H3+ signature of Saturn's 'ring rain'. Geophys. Res. Lett. 44. doi:10.1002/2017GL075932.

Prangé, R., Fouchet, T., Courtin, R., Connerney, J.E.P., McConnell, J.C., 2006. Latitudinal variation of Saturn photochemistry deduced from spatially-resolved ultraviolet spectra. Icarus 180, 379–392. doi:10.1016/j.icarus.2005.11.005.

Richards, P., Fennelly, J., Torr, D., 1994. EUVAC: A solar EUV flux model for aeronomic calculations. J. Geophys. Res. 99 9981-8992.

Rishbeth, H., Mueller-Wodarg, I.C.F., 1999. Vertical circulation and thermospheric composition: a modeling study. Ann. Geophys. 17, 794–805.

Rishbeth, H., Garriott, O., 1969. Introduction to Ionospheric Physics. Academic Press, London.

Rishbeth, H., Mendillo, M., 2001. Patterns of F2-layer variability. J. Atmos. Solar Terr. Phys. 63, 1661–1680.

Rishbeth, H., Mendillo, M., 2004. Ionospheric layers at Earth and Mars. Planet. Space Sci. 52, 849–852. doi:10.1016/j.pss.2004.02.007.

Schunk, R., Nagy, A., 2009. IONOSPHERES: Physics. Plasma Physics and Chemistry, 2nd ed. Cambridge Univ. Press, Cambridge, UK.

Smith, H.T., Johnson, R.E., Perry, M.E., Mitchell, D.G., McNutt, R.L., Young, D.T., 2010. Enceladus plume variability and the neutral gas densities in Saturn's magnetosphere. J. Geophys. Res. Space Phys. 115 (10), 1–11. doi:10.1029/2009JA015184.

Stallard, T., Lystrup, M., Miller, S., 2008a. Emission-line imaging of Saturn's H3+ aurora. Astrophys. J. 675, 117–120.

Stallard, T., Miller, S., Lystrup, M., Achilleos, N., Bunce, E.J., Arridge, C.S., Dougherty, M.K., Cowley, S.W.H., Badman, S.V, Talboys, D.L., Brown, R.H., Baines, K.H., Buratti, B.J., Clark, R.N., Sotin, C., Nicholson, P.D., Drossart, P., 2008b. Complex structure within Saturn's infrared aurora. Nature 456 (7219), 214–217. doi:10.1038/nature07440.